

## Flexible Superlubricity Unveiled in Sidewinding Motion of Individual Polymeric Chains

J. G. Vilhena<sup>1,2,\*</sup>, Rémy Pawlak<sup>1,†</sup>, Philipp D'Astolfo<sup>1</sup>, Xunshan Liu<sup>3,4</sup>, Enrico Gnecco<sup>5</sup>, Marcin Kisiel<sup>1</sup>, Thilo Glatzel<sup>1</sup>, Rúben Pérez<sup>2,6</sup>, Robert Häner<sup>4</sup>, Silvio Decurtins<sup>4</sup>, Alexis Baratoff<sup>1</sup>, Giacomo Prampolini<sup>7</sup>, Shi-Xia Liu<sup>4</sup>, and Ernst Meyer<sup>1,‡</sup>

<sup>1</sup>Department of Physics, University of Basel, Klingelbergstrasse 82, 4056 Basel, Switzerland

<sup>2</sup>Departamento de Física Teórica de la Materia Condensada, Universidad Autónoma de Madrid, E-28049 Madrid, Spain

<sup>3</sup>Department of Chemistry, Zhejiang Sci-tech University, Hongzhou, China

<sup>4</sup>Department of Chemistry, Biochemistry and Pharmaceutical Sciences, University of Bern, Freiestrasse 3, 3012 Bern, Switzerland

<sup>5</sup>Marian Smoluchowski Institute of Physics, Jagiellonian University, Lojasiewicza 11, 30-348 Krakow, Poland

<sup>6</sup>Condensed Matter Physics Center (IFIMAC), Universidad Autónoma de Madrid, E-28049 Madrid, Spain

<sup>7</sup>CNRConsiglio Nazionale delle Ricerche, Istituto di Chimica dei Composti Organo Metallici (ICCOM-CNR) Pisa, Italy

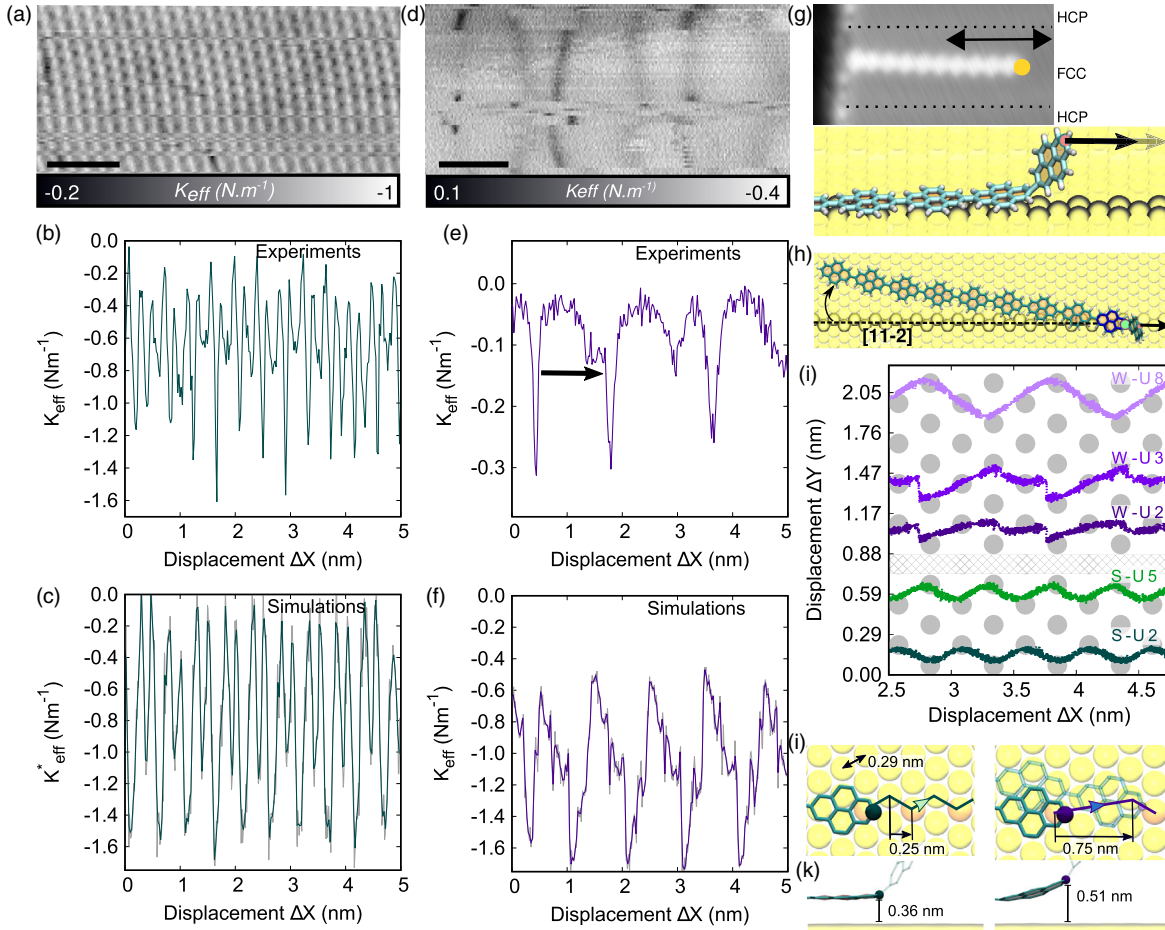
(Received 28 September 2021; revised 22 February 2022; accepted 19 April 2022)

A combination of low temperature atomic force microscopy and molecular dynamic simulations is used to demonstrate that soft designer molecules realize a sidewinding motion when dragged over a gold surface. Exploiting their longitudinal flexibility, pyrenylene chains are indeed able to lower diffusion energy barriers via on-surface directional locking and molecular strain. The resulting ultralow friction reaches values on the order of tens of pN reported so far only for rigid chains sliding on an incommensurate surface. Therefore, we demonstrate how molecular flexibility can be harnessed to realize complex nanomotion while retaining a superlubric character. This is in contrast with the paradigm guiding the design of most superlubric nanocontacts (mismatched rigid contacting surfaces).

DOI:

Controlling friction is arguably one of the oldest quests of our civilization [1,2]. From wetting the desert sands to transport the building block of ancient Egyptian wonders [3] down to micro-electro-mechanical devices [4], a better understanding of this ubiquitous phenomena has closely followed our technological advancement. Thus, the realization of a near frictionless sliding contact [5,6], known as structural superlubricity, has attracted a widespread interest [4,7–12]. Structural superlubricity emerges from a lattice mismatch or misalignment between two sliders in direct contact ultimately preventing them from interlocking—thus reducing energy barriers related to lateral motion. Hence, superlubric designs depend on the sliders' rigidity [4] to prevent the geometrical registry naturally favored by the interaction between contacts—a stringent criteria often leading to its demise [4]. Concomitantly, recent trends in nanodevices depart from the use of rigid elements to embrace bioinspired designs [13], where flexibility is pivotal for the device function [13–16]. Here we explicitly challenge the importance of rigidity in superlubricity by recognizing ultralow friction in the sidewinding [17–19] motion of a molecular system. We also show how *flexolubricity* is achieved by means of complex on-surface dynamics, which goes well beyond rectilinear nanomotion and paves the way for improved energy dissipation schemes in novel molecular architectures and future nanobionic devices.

Purposely synthesized 2,7-dibromopyrene monomers (DBP) are evaporated onto a clean Au(111) crystal and subsequently polymerized *via* Ullmann coupling. The resulting flexible chains are imaged using a combined scanning tunneling microscope (STM) and atomic force microscope (AFM) operated at low temperature (4.8 K) and ultra-High-Vacuum (UHV) [20]. The chain manipulation is achieved thanks to a stable tip-molecule bound formed by pressing the AFM tip against one end of a chain [yellow dot in Fig. 1(g)] [7,32–34]. During the manipulation, the tip kept oscillating at an amplitude of 50 pm and eigenfrequency  $f_0$  of the supporting qPlus tuning fork. The measured frequency shifts  $\Delta f$  directly relates to the gradient of the normal force acting on the tip,  $k_{\text{eff}}$  [32,35]. Although not trivially connected to friction forces,  $k_{\text{eff}}$  informs [4,7,9] about the dynamics (e.g., slip length, hysteresis,...) and it may be computed using all atom molecular dynamics (MD) [7,33,34]. Here, an atomic detailed understanding on the link between flexibility and superlubricity is provided by MD simulations of a 10-unit pyrenylene chain (polymer of 10 DBP units) adsorbed along  $[11\bar{2}]$  crystallographic direction of a Au(111) surface. The chain is then manipulated (first lifted, then sled along  $[11\bar{2}]$ ) at a speed of 0.1 m/s whilst maintaining a 5 K temperature thanks to a Langevin thermostat [36]. Beyond the atomic details, MD also provided friction and normal forces, and the gradient of



F1:1 FIG. 1. Slithering dynamics of a deca-pyrenylene on Au(111). Experimental stiffness maps  $k_{eff}(x, y)$  (a),(d) representative trace (b),(e)  
 F1:2 and corresponding simulation results (c),(f) obtained during the sliding at different heights, i.e., in strong contact (a)–(c) and in a weak  
 F1:3 contact (d)–(f) regimes. (g) Initial configuration of the polymer before sliding, and schematic side view representation. (h) Representative  
 F1:4 configuration of the deca-pyrenylene during sliding. (i) Paracarbon atom trajectory of the second and fifth units for the strong contact  
 F1:5 regime (S-U2, S-U5 shown in green) and trajectories of the second, third, and eighth units for the weak contact regime (W-U2, W-U3,  
 F1:6 W-U8 shown in purple). Top (j) and side (k) views of intermediate sliding stages in the strong (left) and weak (right) contact regimes.

78 the latter directly relates to experiments data (i.e.,  $k_{eff}$ ). MD  
 79 simulations were carried out using GROMACS-2018.2 [21],  
 80 a purposely derived quantum mechanical force field (QM-  
 81 FF) for the pyrene chain [20], and GolP [22] FF for the  
 82 molecule-gold interaction.

83 Figure 1 shows a 10-unit pyrenylene chain initially  
 84 aligned along the  $[11\bar{2}]$  direction of Au(111) prior to  
 85 manipulation. Conveniently, this spontaneous adsorption  
 86 alignment [33] allows manipulating the molecule without  
 87 crossing a Au(111) herringbone [7]. After its synthesis, the  
 88 molecule is lifted from the surface up to a well-defined  
 89 height  $Z$  and driven for 10 nm along the same  $[11\bar{2}]$   
 90 direction. Figures 1(a) and 1(d) show two representative  
 91  $k_{eff}$  maps obtained by driving the chain head along a series  
 92 of lines parallel to  $[11\bar{2}]$  at low and high tip-sample  
 93 separations ( $Z$ ), respectively,—henceforth referred to as  
 94 strong (low- $Z$ ) and weak (high- $Z$ ) contact regimes (data at  
 95 other heights is provided in Figs. S1–S2 of Ref. [20]).

The strong contact regime is characterized by a  $k_{eff}$  96  
 97 repetition distance of  $d_{SC} = 0.22$  nm [Fig. 1(b)]. Prior  
 98 works [7,32–34] allow us to associate  $k_{eff}$  increase or  
 99 decrease with pinning or unpinning events of the molecule  
 100 to the substrate. However, the measured slip distance  
 101 ( $d_{SC} \sim 0.22$  nm) is much smaller than any substrate’s  
 102 periodicity (i.e.,  $d_{Au-Au} = 0.28$  nm Au-Au distance and  
 103  $d_{[11\bar{2}]} = 0.5$  nm the lattice periodicity along  $[11\bar{2}]$ ). The  
 104 results of all-atom MD simulations are in quantitative  
 105 agreement with experiments [Fig. 1(c)]. Simulations con-  
 106 firm that  $k_{eff}$  maxima or minima are associated with stick or  
 107 slip events and the short sliding period, i.e.,  $d_{SC} < d_{Au-Au}$ ,  
 108 provides a distinct signature of a nontrivial zigzag motion  
 109 shown in the Supplemental Material, video S1 [20].

110 When the pyrenylene head is pulled, the entire chain  
 111 twists its longitudinal axis by  $10^\circ$ – $13^\circ$  with respect to the  
 112 sliding direction [Fig. 1(h)]. At the same time, each  
 113 pyrenylene zigzags forward on the surface by moving only

114 along compact or superlubric directions [23] oriented at  
 115  $\pm 30^\circ$  with the sliding direction—a process known as  
 116 directional locking [4,24,25]. This is apparent in its on-  
 117 surface trajectory [Figs. 1(i),1(j)], where one observes that  
 118 initially the monomer moves away from the sliding-axis  
 119 only to return in the subsequent slip event, but now one  
 120 crystallographic position ahead along the sliding direction  
 121 (i.e.,  $d_{[11\bar{2}]} = 0.5 \text{ nm} \approx 2 \times d_{SC}^{MD}$ ). This intermediate off-  
 122 axis slide event, not only explains the small slip distance  
 123  $d_{SC}$  but it also proves the existence of a molecular  
 124 undulation—in agreement with prior theoretical predictions  
 125 on other chains [12]. Moreover, this sinusoidal motion is  
 126 not a rigid one, instead, it is a dynamic concerted motion  
 127 throughout the chain with a large phase shift between  
 128 neighboring units [see in Fig. 1(i) how the  $n$ th unit  
 129 oscillates in antiphase with the  $(n + 3)$ -th]. In the following  
 130 we explain how this complex motion (that partially  
 131 resembles snake sidewinding motion [17–19]) allows the  
 132 chain to effectively mitigate static and sliding friction.

133 In the weak contact regime, the experimental  $k_{eff}$  map  
 134 [Figs. 1(d) and 1(e)] changes substantially, with short stick-  
 135 slip events being replaced by long and less regular jumps.  
 136 The simulation results in Fig. 1(f), show a  $k_{eff}$  periodicity of  
 137  $d_{WC} \sim 1 \text{ nm}$ —similarly to experiments [arrow in Fig. 1(e)].  
 138 Moreover, each unit advances in a specific way, and  
 139 trajectories of consecutive units are not simply shifted as  
 140 in the case of strong contact [see Fig. 1(i)]. Therefore, a  
 141 small change of pyrenylene head height (of 0.15 nm from  
 142 the strong to weak contact regime) alter the dynamics of a  
 143 9 nm long chain all the way to its tail. This effect arises  
 144 from the torsion between consecutive units, that in the gas  
 145 phase favors a  $40^\circ$  angle (see Fig. S3 [20])—opposed to the  
 146  $\approx 0^\circ$  angle of the adsorbed pyrenylene chain. In the strong-  
 147 contact regime the second unit lays flat and the U2–U3  
 148 torsion is nearly zero. By lifting the second unit 0.15 nm,  
 149 the U2–U3 angle is no longer zero and the torsion between  
 150 these units pushes the molecule away from the sliding axis  
 151 (Fig. S3 [20]). Thus, via a small height change one enables  
 152 or disables an internal coordinate of the molecule, which, in  
 153 turn, allows us to alter the dynamics of the chain as a whole  
 154 (Fig. S3 [20]). Interestingly, a comparable effect (so-called  
 155 “rolling”) is also found in snakes [18].

156 It is also instructing to investigate how molecular  
 157 flexibility, and consequent sideway-zigzag motion, play  
 158 out in a backward manipulation [Fig. 2(a)]. In Figs. 2(b)  
 159 and 2(c) we compare experimental and simulated variations  
 160 of  $k_{eff}$  when the pyrenylene chain is pulled forth and back  
 161 in the strong contact regime. In contrast to superlubric  
 162 graphene-nanoribbon (GNR) sliding over Au(111) [7], here  
 163 only a small hysteresis is observed, suggesting that the  
 164 sliding occurs even more smoothly than in rigid GNRs [7].  
 165 Moreover, a close inspection of the trajectory (see  
 166 Supplemental Material [20], movie 3) reveals that (i) in  
 167 spite of its high in-plane flexibility, the molecule slides  
 168 back with the tail moving ahead [Fig. 2(c)]; and (ii) the

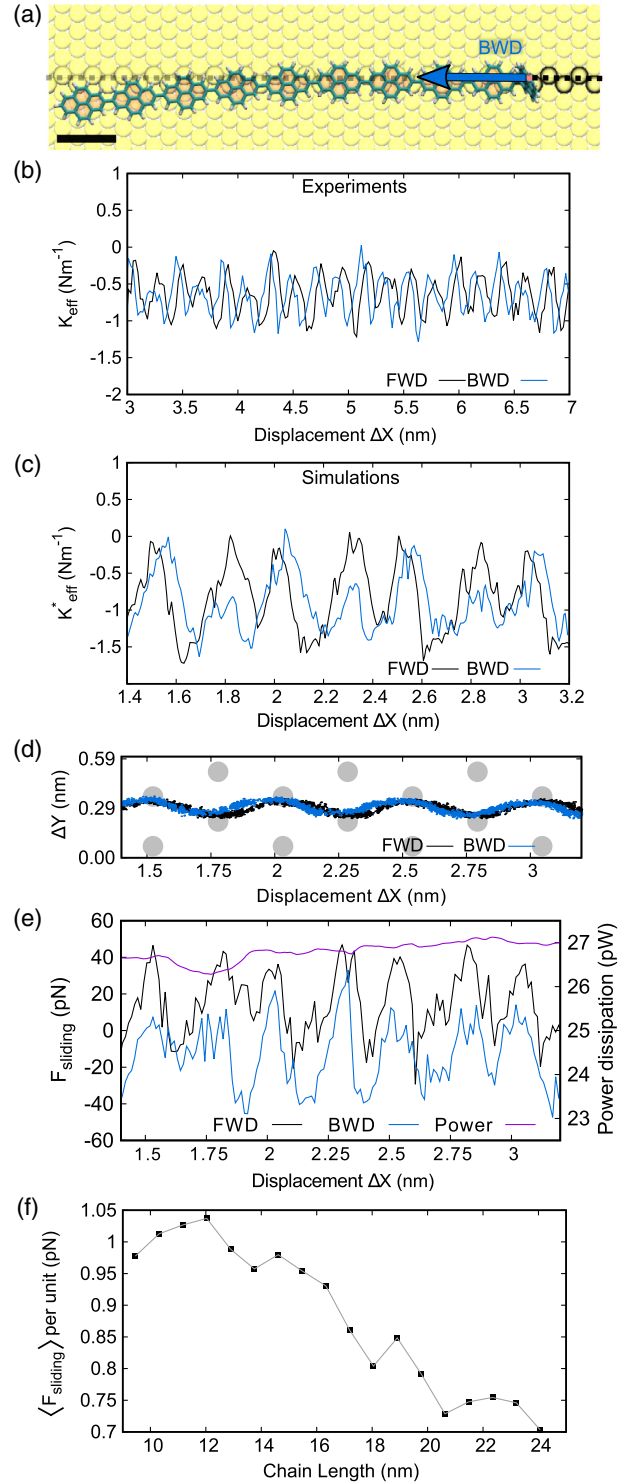


FIG. 2. Backward sliding and apparent flexible superlubricity. (a) Representative snapshot of the backward motion of the deca-pyrenylene. (b),(c) Forward (FWD) and backward (BWD)  $k_{eff}(x)$  obtained in experiments and simulations, respectively. (d) Unit 2 para-carbon atom trajectory of the deca-pyrenylene FWD/BWD sliding. (e) FWD/BWD deca-pyrenylene sliding force traces with the corresponding power dissipation. (f) Average friction per unit as a function of the poly-pyrenylene chain length.

F2:1  
 F2:2  
 F2:3  
 F2:4  
 F2:5  
 F2:6  
 F2:7  
 F2:8  
 F2:9

169 wavy motion at the single pyrenylene level is preserved  
 170 regardless of the sliding direction, i.e., forward or back-  
 171 ward. Moreover, the motion of the first contact unit is  
 172 almost identical in both directions [Fig. 2(d)], consistently  
 173 with the small  $k_{\text{eff}}$  hysteresis.

174 From the lateral force in Fig. 2(e) we compute a static  
 175 friction of  $F_{\text{stat}} = \sim 40$  pN, which is comparable to super-  
 176 lubric GNR ( $F_{\text{stat}}^{\text{GNR}} \sim 35$  pN) sliding along a more packed or  
 177 lubric [23] direction. Therefore our results show that  
 178 ultralow friction is not exclusive to rigid sliders [7–9,11]  
 179 as it may also be realized in flexible ones. Moreover, the  
 180 slider rigidity has also guided most of today’s superlubric  
 181 designs [4,7,8,10,11], as it prevents establishing a geo-  
 182 metric registry with the surface lattice—thus canceling  
 183 friction forces. One hallmark feature of standard super-  
 184 lubric contacts is the asymptotically vanishing friction  
 185 per unit area of contact—a property verified in GNR  
 186 with lengths up to 25 nm [7]. In Fig. 2(f), we represent  
 187 the simulated average sliding friction as a function of the  
 188 number of pyrene units. As in superlubric GNRs, the  
 189 sliding friction is found to decrease with increasing chain  
 190 length. A similar conclusion holds for static friction  
 191 (Fig. S4 [20]), meaning that the energy required to unpin  
 192 a given chain atom is reduced by increasing pyrenylene  
 193 chain length. In a chain capable of improving its registry in  
 194 every slip event—ergo incompatible with conventional  
 195 structural-superlubricity [4,7,8,10,11]—such force cancel-  
 196 lation must stem from internal molecular forces.

197 In the following we thus focus on the incommensurability  
 198 between polycyclic-aromatic-hydrocarbon chains and  
 199 Au(111). It causes two major effects: (i) mechanical stress  
 200 due to surface-templated bending, and (ii) “asynchronous”  
 201 excitation or deexcitation of internal degrees of freedom  
 202 (DOF) while sliding. The first effect is revealed by the angle  
 203 between the first and second adsorbed units in the strong  
 204 contact regime [Fig. 3(a)]. This angle oscillates between two  
 205 nonequilibrium values ( $\pm 0.75^\circ$ ), corresponding to initial and  
 206 intermediate bent states. Consequently, the chain is con-  
 207 stantly under strain except when it slips from one configu-  
 208 ration to another [highlighted by a purple dashed line in  
 209 Figs. 3(a)–3(c)]. The second effect is less local, as exem-  
 210 plified in Fig. 3(a) when comparing the bend angles of the  
 211 U2–U3 and U5–U6 junctions. Upon sliding, these angles  
 212 oscillate almost in antiphase thus canceling out much of the  
 213 lateral forces. However, two perfectly synchronized bending  
 214 events throughout the whole chain are never observed,  
 215 regardless the chain length (Fig. S5 [20]). Therefore, the  
 216 chain is constantly under strain while sliding with internal  
 217 DOF being continuously excited or deexcited. As a result,  
 218 the chain length can be virtually increased without propor-  
 219 tionally increasing the work required to bend all units (see  
 220 Supplemental Material [20], note 2 for details). In other  
 221 words, the incommensurability between pyrenylene and  
 222 Au(111), induces local bending with spatially incoherent  
 223 phase shifts among the pyrenylene units inasmuch as atomic

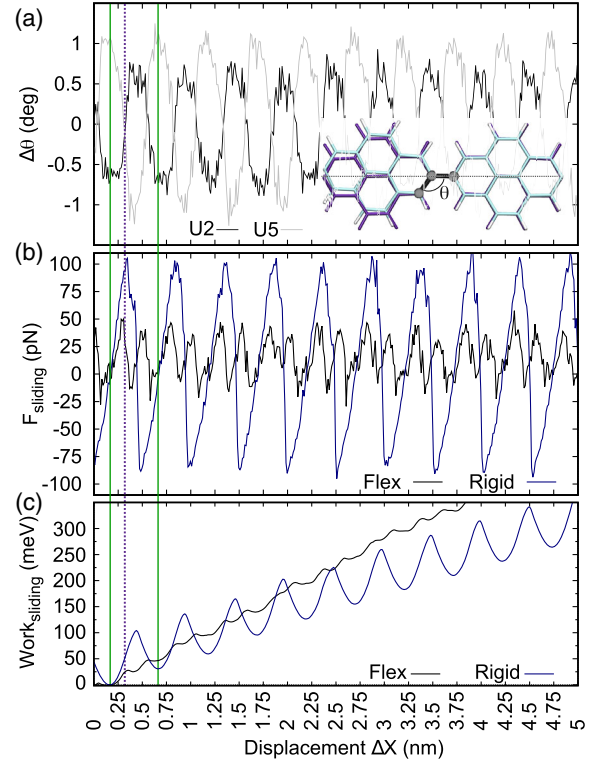


FIG. 3. Correlation between excitation of bending angles, slip  
 dynamics, and energy dissipation of a deca-pyrenylene sled over  
 Au(111). (a) Evolution of  $\Delta\theta$  during sliding [U2 stands for unit  
 2 and 3, and U5 for unit 5 and 6—trajectories are shown in Fig. 1(i)].  
 In the inset, the bending angle ( $\Delta\theta$ ) between the second and third  
 unit is represented (purple or cyan represent a straight or bent  
 configuration during slip or stick). (b) Evolution of the friction  
 force (c) and work required to displace the chain during the sliding  
 dynamics.

positions of substrate and slider never match in structural  
 superlubricity [4,7,8,10,11].

The role of internal DOF is best seen when comparing  
 friction forces of both flexible and rigid pyrenylene chains  
 sled over Au(111) [Fig. 3(b)]. Three major differences  
 are observed, namely, flexible sideways-zigzag motion:  
 (i) decreases the slip length; (ii) substantially decreases  
 the static-friction force; and (iii) has a higher average-  
 friction force. Regarding the slip length, the rigid chain,  
 lacking the ability to bend, can only slip a distance of  
 $2 \times d_{\text{SC}}$  along the driving direction. From here it follows  
 the first important consequence of molecular flexibility, i.e.,  
 to break down on-surface motion into smaller slip events  
 with smaller energy barriers. The connection with the  
 second observation is straightforward: smaller slip events  
 require unpinning a smaller number of atoms, thus requir-  
 ing lower forces to initiate the motion. Furthermore, the  
 total strain stored in a flexible molecule emerging from the  
 surface templated bending, cannot be recovered in the rigid  
 case. As shown in Fig. 3(a), the bending strain decreases at  
 the onset of slip events only, when the chain is partially

F3:1  
 F3:2  
 F3:3  
 F3:4  
 F3:5  
 F3:6  
 F3:7  
 F3:8  
 F3:9

224  
 225  
 226  
 227  
 228  
 229  
 230  
 231  
 232  
 233  
 234  
 235  
 236  
 237  
 238  
 239  
 240  
 241  
 242  
 243  
 244

245 straightened. Thus, bending energy allows us, on the one  
 246 hand, to reduce the amount of work required to unpin  
 247 pyrenylene atoms, and, on the other, to recover part of the  
 248 slip kinetic energy as molecular strain after the slip (see  
 249 other energy components in Fig. S7 [20]). Nevertheless,  
 250 internal DOF excitation will result in vibrations that couple  
 251 to the substrate and increase energy dissipation, as shown in  
 252 Fig. 3(c). In the rigid case, after each slip event one recovers  
 253 a substantial amount of the energy spent to initiate the  
 254 motion—at odds with the flexible chain, where less than  
 255 10% is recovered. To sum up, the molecular flexibility  
 256 reduces diffusion energy barriers by introducing new local  
 257 minima and controlled release or storage of molecular  
 258 strain. Therefore, flexible chains might outperform rigid  
 259 ones in nanoscale displacements since their diffusion  
 260 energy barriers are substantially reduced.

261 In conclusion, we have shown how molecular flexibility  
 262 can be harnessed to realize complex nanoscale motion,  
 263 while retaining superior tribological performance. The  
 264 sideways-zigzag motion of the chains, the ability to change  
 265 their trajectory by an incremental chain-head lift, its  
 266 flexible-superlubric character, unveiled a rich phenomenol-  
 267 ogy showcasing a great potential in chemically tailoring  
 268 tribological properties of molecules composing the increas-  
 269 ing number of nanomechanical systems [13,15,16]. Most  
 270 importantly, our results demonstrate how superlubricity can  
 271 be realized in flexible contacts—contrary to the pervasive  
 272 paradigm reliant on mismatched rigid contacting surfaces.

273 **4** The work is supported by Swiss National Science  
 274 Foundation (SNF Grant No. CRSK-2 190731/1), Swiss  
 275 Nanoscience Institute (SNI), European Research Council  
 276 (ERC), under the European Unions Horizon 2020 research  
 277 and innovation program (Grant Agreement No. 834402),  
 278 the FET-Open Programme (Grant No. 828966), MSC  
 279 Action DLV-795286, COST Action MP1303, Spanish  
 280 Research Agency (Projects No. MDM-2014-0377,  
 281 No. MAT2014-54484-P, No. MAT2017-83273-R,  
 282 No. PID2020-113722RJ-I00, No. 2020-T1/ND-20306).

285  
 286

\*Corresponding author.  
 guilhermevilhena@gmail.com

†Corresponding author.  
 remy.pawlak@unibas.ch

‡Corresponding author.  
 ernst.meyer@unibas.ch

§These two authors contributed equally.

- 293 **5** [1] D. Dowson, *History of Tribology* (Addison-Wesley Longman  
 294 Limited, Reading, MA, 1978).  
 295 **6** [2] A. Vanossi, N. Manini, M. Urbakh, S. Zapperi, and E.  
 296 Tosatti, Colloquium: Modeling friction: From nanoscale to  
 297 mesoscale, *Rev. Mod. Phys.* **85**, 529 (2013).  
 298 [3] A. Fall, B. Weber, M. Pakpour, N. Lenoir, N. Shahidzadeh,  
 299 J. Fiscina, C. Wagner, and D. Bonn, Sliding Friction on Wet  
 300 and Dry Sand, *Phys. Rev. Lett.* **112**, 175502 (2014).

- [4] A. Vanossi, C. Bechinger, and M. Urbakh, Structural **8** 301  
 lubricity in soft and hard matter systems, *Nat. Commun.*  
**11**, 4657 (2020). 302  
 [5] M. Hirano, K. Shinjo, R. Kaneko, and Y. Murata, 303  
 Anisotropy of Frictional Forces in Muscovite Mica, *Phys.*  
*Rev. Lett.* **67**, 2642 (1991). 304  
 [6] J. M. Martin, C. Donnet, T. Le Mogne, and T. Epicier, 305  
 Superlubricity of molybdenum disulphide, *Phys. Rev. B* **48**,  
 10583 (1993). 306  
 [7] S. Kawai, A. Benassi, E. Gnecco, H. Söde, R. Pawlak, X.  
 Feng, K. Müllen, D. Passerone, C. A. Pignedoli, P. Ruffieux,  
 R. Fasel, and E. Meyer, Superlubricity of graphene nano-  
 ribbons on gold surfaces, *Science* **351**, 957 (2016). 307  
 [8] Y. Song, D. Mandelli, O. Hod, M. Urbakh, M. Ma, and Q.  
 Zheng, Robust microscale superlubricity in graphite/  
 hexagonal boron nitride layered heterojunctions, *Nat. Mater.*  
**17**, 894 (2018). 308  
 [9] O. Hod, E. Meyer, Q. Zheng, and M. Urbakh, Structural 309  
 superlubricity and ultralow friction across the length scales,  
*Nature (London)* **563**, 485 (2018). 310  
 [10] D. Dietzel, J. Brndiar, I. Štich, and A. Schirmeisen, 311  
 Limitations of structural superlubricity: Chemical bonds  
 versus contact size, *ACS Nano* **11**, 7642 (2017). 312  
 [11] S. Zhang, T. Ma, A. Erdemir, and Q. Li, Tribology of two-  
 dimensional materials: From mechanisms to modulating  
 strategies, *Mater. Today* **26**, 67 (2019). 313  
 [12] W. Ouyang, D. Mandelli, M. Urbakh, and O. Hod, Nano-  
 serpents: Graphene nanoribbon motion on two-dimensional  
 hexagonal materials, *Nano Lett.* **18**, 6009 (2018). 314  
 [13] L. Zhang, V. Marcos, and D. A. Leigh, Molecular machines  
 with bio-inspired mechanisms, *Proc. Natl. Acad. Sci.*  
*U.S.A.* **115**, 9397 (2018). 315  
 [14] Z. Wang, J. Wang, J. Ayarza, T. Steeves, Z. Hu, S. Manna,  
 and A. P. EsserKahn, Bio-inspired mechanically adaptive  
 materials through vibration-induced crosslinking, *Nat. Ma-*  
*ter.* **20**, 869 (2021). 316  
 [15] D. Peller, L. Z. Kastner, T. Buchner, C. Roelcke, F.  
 Albrecht, N. Moll, R. Huber, and J. Repp, Sub-cycle  
 atomic-scale forces coherently control a single-molecule  
 switch, *Nature (London)* **585**, 58 (2020). 317  
 [16] D. Civita, M. Kolmer, G. J. Simpson, A. P. Li, S. Hecht, and  
 L. Grill, Control of long-distance motion of single mole-  
 cules on a surface, *Science* **370**, 957 (2020). 318  
 [17] H. C. Astley, C. Gong, J. Dai, M. Travers, M. M. Serrano,  
 P. A. Vela, H. Choset, J. R. Mendelson, D. L. Hu, and D. I.  
 Goldman, Modulation of orthogonal body waves enables  
 high maneuverability in sidewinding locomotion, *Proc.*  
*Natl. Acad. Sci. U.S.A.* **112**, 6200 (2015). 319  
 [18] H. Marvi, C. Gong, N. Gravish, H. Astley, M. Travers, R. L.  
 Hatton, J. R. Mendelson, H. Choset, D. L. Hu, and D. I.  
 Goldman, Sidewinding with minimal slip: Snake and robot  
 ascent of sandy slopes, *Science* **346**, 224 (2014). 320  
 [19] I. J. Yeaton, S. D. Ross, G. A. Baumgardner, and J. J. Socha,  
 Undulation enables gliding in flying snakes, *Nat. Phys.* **16**,  
 974 (2020). 321  
 [20] See Supplemental Material at [http://link.aps.org/  
 supplemental/10.1103/PhysRevLett.000.000000](http://link.aps.org/supplemental/10.1103/PhysRevLett.000.000000), which in-  
 cludes Refs. [21–31]. 322  
 [21] M. J. Abraham, T. Murtola, R. Schulz, S. Pii, J. C. Smith,  
 B. Hess, and E. Lindahl, Gromacs: High performance 323  
 324  
 325  
 326  
 327  
 328  
 329  
 330  
 331  
 332  
 333  
 334  
 335  
 336  
 337  
 338  
 339  
 340  
 341  
 342  
 343  
 344  
 345  
 346  
 347  
 348  
 349  
 350  
 351  
 352  
 353  
 354  
 355  
 356  
 357  
 358  
 359  
 360

- 361 molecular simulations through multi-level parallelism from  
362 laptops to supercomputers, *SoftwareX* **1–2**, 19 (2015).
- 363 **10** [22] S. C. F. Iori, R. Di Felice, and E. Molinari, GoIP: An  
364 atomistic force-field to describe the interaction of proteins  
365 with Au(111) surfaces in WaterGoIP: An atomistic force-  
366 field to describe the interaction of proteins with Au(111)  
367 surfaces in water, *J. Comput. Chem.* **30**, 1465 (2009).
- 368 [23] L. Gigli, N. Manini, A. Benassi, E. Tosatti, A. Vanossi, and  
369 R. Guerra, Graphene nanoribbons on gold: Understanding  
370 superlubricity and edge effects, *2D Mater.* **4**, 045003 (2017).
- 371 [24] X. Cao, E. Panizon, A. Vanossi, N. Manini, and C.  
372 Bechinger, Orientational and directional locking of colloidal  
373 clusters driven across periodic surfaces, *Nat. Phys.* **15**, 776  
374 (2019).
- 375 [25] F. Trillitzsch, R. Guerra, A. Janas, N. Manini, F. Krok, and E.  
376 Gnecco, Directional and angular locking in the driven motion  
377 of Au islands on  $\text{mos}_2$ , *Phys. Rev. B* **98**, 165417 (2018).
- 378 [26] A. G. Crawford, Z. Liu, I. A. I. Mkhalid, M.-H. Thibault, N.  
379 Schwarz, G. Alcaraz, A. Steffen, J. C. Collings, A. S.  
380 Batsanov, J. A. K. Howard, and T. B. Marder, Synthesis of  
381 2- and 2,7-functionalized pyrene derivatives: An application  
382 of selective C-H borylation, *Chem. Eur. J.* **18**, 5022 (2012).
- 383 [27] F. J. Giessibl, The qPlus sensor, a powerful core for the  
384 atomic force microscope, *Rev. Sci. Instr.* **90**, 011101 (2019).
- 385 [28] S. Páll, M. J. Abraham, C. Kutzner, B. Hess, and E. Lindahl,  
386 Tackling exascale software challenges in molecular dynam-  
387 ics simulations with GROMACS, in *Solving Software Chal-*  
388 *lenges for Exascale*, edited by S. Markidis and E. Laure  
389 (Springer International Publishing, Cham, 2015), pp. 3–27.
- 390 [29] T. Darden, D. York, and L. Pedersen, Particle mesh Ewald:  
391 An  $n \log(n)$  method for Ewald sums in large systems, *J.*  
392 *Chem. Phys.* **98**, 10089 (1993).
- 393 [30] S. Scherb, A. Hinaut, R. Pawlak, J. G. Vilhena, Y. Liu, S.  
394 Freund, Z. Liu, X. Feng, K. Müllen, T. Glatzel, A. Narita,  
and E. Meyer, Giant thermal expansion of a two-dimen- 395  
sional supramolecular network triggered by alkyl chain 396  
motion, *Commun. Mater.* **1**, 8 (2020). 397
- [31] I. Cacelli and G. Prampolini, Parametrization and validation 398  
of intramolecular force fields derived from DFT calcula- 399  
tions, *J. Chem. Theory Comput.* **3**, 1803 (2007). 400
- [32] S. Kawai, M. Koch, E. Gnecco, A. Sadeghi, R. Pawlak, T. 401  
Glatzel, J. Schwarz, S. Goedecker, S. Hecht, A. Baratoff, L. 402  
Grill, and E. Meyer, Quantifying the atomic-level mechanics 403  
of single long physisorbed molecular chains, *Proc. Natl.*  
*Acad. Sci. U.S.A.* **111**, 3968 (2014). 404
- [33] R. Pawlak, J. G. Vilhena, P. D’astolfo, X. Liu, G. 405  
Prampolini, T. Meier, T. Glatzel, J. A. Lemkul, R. Häner, 406  
S. Decurtins, A. Baratoff, R. Pérez, S. X. Liu, and E. Meyer, 407  
Sequential bending and twisting around C-C single bonds 408  
by mechanical lifting of a pre-adsorbed polymer, *Nano Lett.*  
**20**, 652 (2020). 409
- [34] R. Pawlak, J. G. Vilhena, A. Hinaut, T. Meier, T. Glatzel, A. **11** 412  
Baratoff, E. Gnecco, R. Pérez, and E. Meyer, Conformations 413  
and cryo-force spectroscopy of spray-deposited single- 414  
strand DNA on gold, *Nat. Commun.* **10**, 685 (2019). 415
- [35] R. Pawlak, W. Ouyang, A. E. Filippov, L. Kalikhman- 416  
Razvozov, S. Kawai, T. Glatzel, E. Gnecco, A. Baratoff, 417  
Q. Zheng, O. Hod, M. Urbakh, and E. Meyer, Single- 418  
molecule tribology: Force microscopy manipulation of a 419  
porphyrin derivative on a copper surface, *ACS Nano* **10**, 713  
(2016). 420
- [36] N. Goga, A. J. Rzepiela, A. H. de Vries, S. J. Marrink, and 421  
H. J. C. Berendsen, Efficient algorithms for Langevin and 422  
DPD dynamics, *J. Chem. Theory Comput.* **8**, 3637 (2012). 423
- [37] J. Cerezo, G. Prampolini, and I. Cacelli, Developing **12** 425  
accurate intramolecular force fields for conjugated systems 426  
through explicit coupling terms, *Theor. Chem. Acc.* **137**, 80  
(2018). 427  
428  
429